Published in final edited form as:

Proc Combust Inst. 2019 ; 37: . doi:10.1016/j.proci.2018.06.140.

Numerical study of gas-phase interactions of phosphorus compounds with co-flow diffusion flames

Fumiaki Takahashi[*],
Case Western Reserve University, Cleveland, OH 44106, USA

Viswanath R. Katta,
Innovative Scientific Solutions, Inc., Dayton, OH 45440, USA

Gregory T. Linteris,
National Institute of Standards and Technology, Gaithersburg, MD 20899, USA

Valeri I. Babushok
National Institute of Standards and Technology, Gaithersburg, MD 20899, USA

Abstract

The effects of phosphorus-containing compounds (PCCs) on the extinguishment and structure of methane-air coflow diffusion flames, in the cup-burner configuration, is studied computationally. Dimethyl methylphosphonate (DMMP), trimethyl phosphate (TMP), or phosphoric acid is added to either the air or fuel flow. Time-dependent axisymmetric computation is performed with full gas-phase chemistry and transport to reveal the flame structure and inhibition process. A detailed chemical-kinetics model (77 species and 886 reactions) is constructed by combining the methane-oxygen combustion and phosphorus inhibition chemistry. A simple model for radiation from CH_4, CO, CO_2, H_2O, and soot based on the optically thin-media assumption is incorporated into the energy equation. The inhibitor effectiveness is calculated as the minimum extinguishing concentrations (MECs) of CO_2 (added to the oxidizer) as a function of the PCC loading (added to the oxidizer or fuel stream). The calculated MEC of CO_2 without an inhibitor is in good agreement with the measured value. For moderate DMMP loading to the air (<1 %), the measured value becomes significantly smaller, presumably due to particle formation in the experiment. An inhibitor in the oxidizer flow is an order of magnitude more effective compared to that in the fuel flow in gas-phase inhibition of co-flow diffusion flames. The three PCCs studied behave similarly with regard to flame inhibition, lowering radical concentrations and the heat-release rate at the flame-stabilizing peak reactivity spot (i.e., reaction kernel) in the base, promoting flame blow-off. The three compounds behave differently, however, with regard to the trailing flame. While all three raise the maximum temperature in the trailing flame, DMMP and TMP, which contain three methyl groups, result in higher maximum flame temperature and combustion enhancement there, with a unique two-zone flame structure, whereas phosphoric acid does not.

[*]Corresponding Author: Dr. Fumiaki Takahashi, Department of Mechanical and Aerospace Engineering, Case Western Reserve University, 10900 Euclid Avenue, Cleveland, Ohio 44106, USA, Fax: 1 (216) 368-6838, fxt13@case.edu.

Keywords

Fire retardant; Reaction inhibitor; Combustion enhancement; Extinguishment; Cup burner

1 INTRODUCTION

Fire retardants (FRs), used in polymers, textiles, and coatings, are often classified as acting either in the condensed phase or gas phase [1,2]. Gas-phase active FRs have the advantage of working for a variety of polymers, and are very widely used [3]. The most common gas-phase active FR formulations are those containing bromine compounds, with antimony trioxide usually added as a synergist. Due to environmental and health concerns, however, manufactures are moving away from the bromine-based fire retardants. The alternative chemical systems of highest interest to industry and researchers are those containing phosphorus [4,5]. Phosphorus-containing compounds (PCCs) are known to be effective at reducing flammability of polymers [6–8], and their use as FR additives to plastics has increased dramatically in recent years [2,9]. Recent work suggests comparable importance of gas-phase chemistry and solid-phase effects such as char promotion, depending on the specific PCC chemistry [6,10]. PCCs have also been evaluated as potential halon replacements for fire suppression using cup burner, streaming tests [11], and opposed-jet diffusion flames [7]. Further understanding of how PCCs affect flames is important for their efficient use.

A gas-phase chemical kinetics model of phosphorus compounds in flames has been developed [8,12–16]. The decomposition of DMMP (or other PCCs) in a flame is a relatively fast, complicated process occurring near the main reaction zone, leading to the principle intermediate species PO_2, PO, HOPO and $HOPO_2$. These compounds participate in catalytic radical recombination cycles that reduce chain-branching radical concentrations from super-equilibrium to equilibrium levels, and hence inhibit the flame. Sensitivity and reaction pathway analyses reveal two main inhibition cycles, uncovered previously [newref1], as shown in Table 1. Each step in these cycles involves scavenging of H, O, or OH radicals, which decreases their concentration and the overall reaction rate of the flame. Although this mechanism has been used to model the inhibition of premixed and counterflow diffusion flames with reasonable results [17–21], no researchers have extensively studied co-flow diffusion flames, for which poor performance has been observed [7].

The effectiveness of compounds in gaseous flame inhibition is quite complex, and it depends upon the additive type as well as flame properties. For example, Dimethylmethylphosphonate (DMMP, $PO[CH_3][OCH_3]_2$) is about 141 times as effective as CO_2 in a premixed flame [22], 30 times as effective in a counter-flow diffusion flame [7] but only 3 times as effective in a cup-burner flame [23]. For phosphorus, this large variation in effectiveness with flame type has not been explained. Since phosphorous is and will be used as a gas-phase active FR, it would be of great value to understand the conditions for which it is effective.

Recent experiments have studied DMMP in methane cup-burner flames [24]. The inhibitor effectiveness was measured as the minimum extinguishing concentrations (MECs) of CO_2 (added to the oxidizer) as a function of the DMMP loading (added to the oxidizer or fuel stream, both at 295 K); similar results were found with n-heptane as the fuel [25]. Previous work has computationally investigated various fire suppressants added to cup-burner flames [26–28]. The present paper calculates the effects of three PCCs: DMMP, tetramethylphosphate (TMP, $PO[OCH_3]_3$), or phosphoric acid ($PO[OH]_3$), added to the oxidizer or fuel flow. The overall goal of the present work is to understand how the properties of flames interact with the gas-phase inhibition to influence the agent effectiveness. The knowledge of detailed flame structure will help to uncover the reasons for the variation of effectiveness of phosphorus with flame type, and to shed light on how gas-phase acting fire retardants actually retard ignition or reduce heat release. Ultimately, this work aims to aid in the development or application of new compounds to be used as flame retardants in high-volume thermoplastics.

2 COMPUTATIONAL METHODS

A time-dependent, axisymmetric numerical code (UNICORN) [29,30] is used for the simulation of diffusion flames stabilized on the cup burner. The code solves the axial and radial (z and r) full Navier-Stokes momentum equations, continuity equation, and enthalpy- and species-conservation equations on a staggered-grid system. A clustered mesh system is employed to trace the gradients in flow variables near the flame surface. The thermophysical properties such as enthalpy, viscosity, thermal conductivity, and binary molecular diffusion of all species are calculated from the polynomial curve fits for the temperature range 300 K to 5000 K. Mixture viscosity and thermal conductivity are estimated using the Wilke and Kee expressions, respectively. Molecular diffusion is assumed to be of the binary-diffusion type, and the diffusion velocity of a species is calculated using Fick's law and the effective-diffusion coefficient of that species in the mixture. A simple radiation model based on the optically thin-media assumption is incorporated into the energy equation. Radiation from CH_4, CO, CO_2, H_2O and soot is considered.

A comprehensive reaction mechanism is assembled and integrated into the UNICORN code for the simulation of methane flames with a PCC. The mechanism (77 species and 886 elementary reactions) contains a sub-mechanism for methane-oxygen combustion (GRI-V3.0 [31]) and for phosphorus species flame reactions [32] (41 species and 448 reactions).

The finite-difference forms of the momentum equations are obtained using an implicit QUICKEST scheme [33], and those of the species and energy equations are obtained using a hybrid scheme of upwind and central differencing. At every time-step, the pressure field is accurately calculated by solving all the pressure Poisson equations simultaneously and using the LU (Lower and Upper diagonal) matrix-decomposition technique.

Unsteady axisymmetric calculations for the cup-burner flames are made on a physical domain of 200 mm by 47.5 mm using a 351×151 non-uniform grid system that yields 0.2 mm×0.15 mm minimum grid spacing in the z and r directions, respectively, in the flame zone. The computational domain is bounded by the axis of symmetry and chimney wall

boundary in the radial direction and by the inflow and outflow boundaries in the axial direction. The outflow boundary in z direction is located sufficiently far from the burner exit (~14 fuel-cup radii) such that propagation of boundary-induced disturbances into the region of interest is minimal. Flat velocity profiles are imposed at the fuel and air inflow boundaries, while an extrapolation procedure with weighted zero- and first-order terms is used to estimate the flow variables at the outflow boundary. The cup burner outer diameter is 28 mm and the chimney inner diameter is 95 mm. The burner wall (1-mm long and 1-mm thick tube) temperature is set at 600 K, and the wall surface has the no-slip velocity condition. The mean gas velocities of the fuel (methane) and oxidizer streams are 1.24 cm/s and 15.5 cm/s, respectively, and their temperature, 374 K. The low fuel velocity represents low momentum conditions typical of condensed material fires. The air velocity is in the middle of the so-called “plateau region [27]”, where the extinguishing agent concentration is independent of the oxidizer velocity. The computational conditions are selected to match those of the experiments used for comparisons [24].

Validation of the UNICORN code has been performed for a variety of flame systems, fuels, and inhibitors with the kinetic model used. For the case of DMMP, the present work predicts global strain rates at extinction of methane-air opposing-jet flames at the reactant temperature of 100 °C to be 380 s^{-1} without the inhibitor, which is close to the measured value (360 s^{-1}) [7], and those with DMMP, to be within 10% of the experiments, for a variety of stretch rates [7].

3 RESULTS AND DISCUSSION

3.1 Minimum Extinguishing Concentration (MEC)

To determine the effectiveness of the PCCs in extinguishing the cup-burner flame, stable flames are calculated first by increasing incrementally (starting at 0) the loading of each PCC in the oxidizer or fuel stream. Then, the flame extinguishing conditions with CO_2 are determined by increasing the CO_2 volume fraction (X_{CO2}) in the oxidizer (starting at 0; in increments gradually reduced to <1% of X_{CO2} as the limit approached) until the flame blows off. The process is repeated at different PCC loadings.

Figure 1 shows the calculated and measured [24] inhibitor effectiveness expressed as the MECs of CO_2 added to the oxidizer as a function of the PCC loading, when added to the flow of: (a) oxidizer or (b) fuel. The calculated MEC of CO_2 without PCC is X_{CO2}=0.1985, which is in reasonable agreement (≈7%) with the measurement (0.185 at 100°C) [24]. With addition of DMMP to the oxidizer (Fig. 1a) at very low volume fractions ($X_{DMMP,OX}$<0.002), both measured and calculated MECs of CO_2 decrease rapidly, thus indicating excellent suppression effectiveness of DMMP. The concave upward extinguishing-limit curves suggest a synergistic effect by DMMP and CO_2 added together to the oxidizer. The experimental value of MEC of CO_2 decreases more steeply and thus is significantly smaller than the calculated value for 0.002<$X_{DMMP,OX}$<0.007. As the DMMP volume fraction increases further, the rate of decrease (slope) of the MEC curves decreases, particularly for the experiment, and thus the two curves cross at $X_{DMMP,OX}$=0.012. The differences between the measured and calculated MECs are likely due to particle formation,

observed [24] on the air side of the flame zone with DMMP, which is not taken into account in the calculation.

In the experiment [24], the marginal effectiveness of the DMMP diminishes, and for $X_{DMMP,OX}>0.07$, the additional DMMP is essentially ineffective, a result similar to that of metallic compounds added to cup-burner flames [26]. The loss of effectiveness for the metals is believed to be due to particle formation (which act as a sink for the active gas-phase intermediate species that catalytically recombined radicals) [26]. With added DMMP, however, particle formation is outside (upstream) of the main reaction zone [24]. It is possible that the actual flame temperature is lower than the calculated value because of radiative heat loss from the high-temperature particles, thus lowering X_{CO2} for extinguishment. Moreover, premixed flame structure calculations for the reaction kernel [24] implied that DMMP addition reduced the concentrations of the chain-carrier radicals (H, O, and OH) in the premixed-like flame base to the equilibrium levels so that additional DMMP had little effect on the flame.

The calculated MEC of CO_2 for TMP follow closely that for DMMP, while that for phosphoric acid are lower (i.e., higher inhibition effectiveness) at higher volume fractions ($X_{PO[OH]3,OX}>0.005$). The concentration profiles of the main decomposition products (PO_2, HOPO and $HOPO_2$) (not shown) are nearly the same for DMMP and TMP. Unlike DMMP and TMP, which have a significant heating value due to three methyl groups attached to the phosphorus atom, phosphoric acid provides chemical inhibition without the fuel effect. The calculated MECs of DMMP, TMP, and phosphoric acid without CO_2 are 0.018, 0.020, and 0.012.

In the simulation, the inhibitor effectiveness of PCCs is reduced by an order of magnitude when added to the fuel stream (Fig. 1b) as compared to the air stream. As the DMMP volume fraction in the fuel stream increases, the measured [24] MEC of CO_2 added to the oxidizer decreases and DMMP becomes nearly ineffective ($X_{CO2}\approx0.15$) for $0.01<X_{DMMP,FU}<0.04$ (particle formation prevented measurements at higher DMMP loadings). In contrast to air-side addition, fuel-side addition reduces the calculated MEC of CO_2 added to the oxidizer linearly, thus showing no synergistic effect. The MEC of DMMP without CO_2 is 0.281, which is 15.5 times larger than that for the addition to the oxidizer (0.0181).

The calculated MEC of CO_2 added to the oxidizer for TMP added to the fuel follows closely that for DMMP for $X_{TMP,FU}<0.14$, while that for phosphoric acid becomes lower at $X_{PO[OH]3,FU} \approx 0.1$. At higher volume fractions of TMP or phosphoric acid, it was not possible to obtain a numerical solution (due to stiffness in the computation with the phosphorus mechanism); the points connected with dashed lines in Fig. 1b indicate approximate solutions as close to convergance as we could get.

3.2 Flame Structure

The numerical simulations reported previously [33,34] revealed that the premixed-like flame-base region controlled the flame attachment, detachment, and oscillation processes, and also supported the trailing diffusion flame, consistent with the present results. Figure 2

shows the calculated structure of near-extinguishment flames with a PCC added to the oxidizer (without CO_2). The variables include the velocity vectors ($\boldsymbol{v}$), isotherms (T), and heat-release rate ($\dot{q}$). The velocity vectors show the longitudinal acceleration in the hot zone due to buoyancy. Surrounding air is entrained into the lower part of the flame, which inclines inwardly.

The heat-release rate contours show a peak reactivity spot (i.e., the reaction kernel [33]) at the flame base, where the chain-carrier radicals (H, O, and OH), as well as heat, diffuse back against the oxygen-rich incoming buoyancy-induced flow, thus promoting chain-branching ($H+O_2 \rightarrow OH+O$) and subsequent vigorous reactions to form the reaction kernel.

The base of the agent-free flame (not shown) is anchored at the burner rim at the height from the burner rim, z_k=0.8 mm, in which z_k is the height of the reaction kernel above the burner rim. As DMMP or TMP is added to the oxidizer (Figs. 2a and 2b, respectively), the maximum flame temperature increases, compared to the neat flame, and the flame base detaches and lifts from the burner rim. The heat-release rate contour shows a weak branch on the oxidizer side extending downstream along the isotherms (between 1100 K and 1600 K) from the reaction kernel. This two-zone flame structure is similar to that observed previously [28] for halon replacement fire-extinguishing agents that also have fuel components. As a result of mixing of the fuel and oxidizer streams, the reaction kernel broadens further laterally, and the two-zone flame structure is formed due to the heat release by the inhibitor itself on the air side of the main hydrocarbon-oxygen reaction zone. By contrast, the flame with phosphoric acid added to the oxidizer (Fig. 2c) shows the main flame zone only.

Figure 3 shows the calculated structure of near-extinguishment-limit flames with a PCC added to the fuel (without CO_2). Despite the high volume fraction ($X_{DMMP,FU}$=0.28) (Fig. 3a), the maximum flame temperature is nearly constant, compared to the neat flame (not shown). The heat-release rate contour has a short branch extending from the reaction kernel downstream on the fuel side under high temperatures (>1100 K). The flame with phosphoric acid added to the fuel (Fig. 3b) has a relatively thin flame zone ($\dot{q}$ contour) with no sign of the fuel-side branch. Thus, the heat-release rate branch with DMMP is caused by the additional heat release due to the fuel effect of DMMP. Unlike the PCC addition to the oxidizer, for which the agent is conveyed into the flame zone by convection as well as diffusion, the effect of its addition to the fuel on the flame structure is limited to the fuel side of the flame base region.

Figure 4 shows the radial variations of calculated temperature and the heat-release rate crossing the reaction kernel at z_k and the trailing flame at $z=z_k+3$ mm in the near-limit flames. The heat-release rate peak (reaction kernel) resides slightly on the oxidizer side of the temperature peak. For DMMP and TMP added to the oxidizer (Fig. 4a), the trailing flame is characterized by “two-zone” structure [28] as evident from two heat-release rate peaks. The inner zone is formed by methane-O_2 combustion, with similar locations for the peak heat-release rate and temperature. The outer zone is formed by exothermic reactions of the agents’ fuel components. For phosphoric acid addition, the outer heat-release peak nearly disappears. Despite an order-of-magnitude larger volume fraction of DMMP or phosphoric

acid added to the fuel stream (Fig. 4b) than that added to the oxidizer (Fig. 4a), the heat-release rate exhibits a single peak with a larger value, particularly in the reaction kernel. Thus, the agent addition to the fuel stream is inefficient in destabilizing the flame.

For the phosphorus-containing species and the chain-carrier radicals (H, O, and OH), Fig. 5 shows the variation of the volume fractions (X_i) with radial position at a height of the reaction kernel. Results are for DMMP or TMP added to the oxidizer stream (Figs. 5a and 5b, respectively) or DMMP added to the fuel stream (Fig. 5c). The flame structure with DMMP and TMP are very similar, except that for DMMP, the volume fraction of HOPO is higher on the oxidizer side of the flame. The agent (DMMP or TMP) in the oxidizer stream (Figs. 5a and 5b) reacts with O_2 and the radicals, fragments, and diminishes in the region surrounding the reaction kernel. As a result, the peak concentrations of species such as $PO(OH)_3$, CH_3PO_2, and $P(OH)_3$ occur in this peripheral region. Relatively high concentrations ($10^{-3}<X_i<10^{-2}$) of active phosphorus intermediates ($HOPO_2$, HOPO, and PO_2) are present in the high-temperature central region, where the peaks of the chain-carrier radicals also occur. Consequently, the afore-mentioned phosphorus inhibition reactions proceed vigorously in the reaction kernel.

In Fig. 5c, despite an order-of-magnitude higher DMMP loading in the fuel as compared to the oxidizer stream (Fig. 5a), the volume fractions of active phosphorus intermediates ($HOPO_2$, HOPO, and PO_2) are significantly lower at the peak heat-release rate (reaction kernel), where the chain-carrier radicals also peak. The DMMP added to the fuel stream has to diffuse across the opposed-flow oxidizer stream to reach the reaction kernel. As a result, the peak volume fraction of DMMP, which leaked onto the oxidizer side is two orders-of-magnitude lower than that added to the oxidizer. The peak H-atom volume fractions across the reaction kernel of the near-limit flames with added DMMP, TMP, or phosphoric acid are nearly the same, $X_h \approx 0.0002$, for loading to the oxidizer, $X_h \approx 0.00024$ for loading to the fuel.

The stoichiometric mixture fraction, determined by the element mass fractions of carbon, hydrogen, and oxygen [35], for a methane-air flame is 0.055. Therefore, to form a stoichiometric mixture, the fuel-stream fluid is reduced by the mixing to its mass fraction of 0.055, whereas the oxidizer fluid is reduced only to 0.945. This implies that a chemical additive to the fuel stream is ≈17 times less effective, on a mass basis, compared to that to the oxidizer. In addition, the small stoichiometric mixture fraction dictates that the flame zone is formed on the oxidizer side of the dividing streamline between the fuel and oxidizer streams. Consequently, the oxidizer flows into the flame zone, and thus the convective and diffusive fluxes of the oxygen and additive to the flame zone are significant. By contrast, the fuel-loaded additive must diffuse into the oxidizer stream to reach the flame zone as described above.

4 CONCLUSIONS

The physical and chemical effects of the phosphorus-containing compounds on the structure and inhibition of methane cup-burner flames is studied computationally. Although the calculated minimum extinguishing concentration of CO_2 with DMMP addition is

reasonable, the experimental value drops faster, probably due to the radiative heat loss from phosphoric acid particles in the experiments (not modeled in the simulation). The effectiveness of PCCs added to the oxidizer is outstanding, particularly at low loadings. Although PCCs in the oxidizer increases the maximum flame temperature in the trailing diffusion flame, they weaken the premixed-like flame attachment point (reaction kernel), thereby inducing flame detachment, lifting, and blowout extinguishment. A two-zone flame structure is predicted, in which the DMMP or TMP reacts with oxidizing species due to the reactions of the inhibitors' fuel-like components. PCCs in the fuel stream are much less effective in gas-phase inhibition of co-flow diffusion flames primarily due to: (1) the small stoichiometric mixture fraction (0.055 for methane), which requires more retardant to affect the flame, (2) the flame location on the oxidizer side of the dividing streamline, which requires the retardant to diffuse (instead of convect) to the flame, and (3) low concentrations of active phosphorus intermediate species ($HOPO_2$, HOPO, PO_2) in the flame stabilizing region where [O], [H], and [OH] peak, thus leading to poor overlap between the active phosphorous compounds and the radicals, which is necessary for the catalytic radical recombination cycle to be effective. The results have important implications for gas-phase active fire retardants, which are always introduced with the fuel.

ACKNOWLEDGMENTS

This work was supported under the Cooperative Agreement by the National Institute of Standards and Technology with FXT Consulting, LLC.

REFERENCES

1. Fenimore CP, Jones GW, Combust. Flame 10 (1966) 295–301.
2. Levchik SV, In: Morgan AB, Wilkie CA (Eds.), Flame Retardant Polymer Nanocomposites, John Wiley & Sons, Inc (2007) 1–29.
3. Linteris GT, Gas-phase mechanisms of fire retardants, NIST IR 6889, National Institute of Standards and Technology (2002).
4. Schartel B, Materials 3 (2010) 4710–4745. [PubMed: 28883349]
5. Levchik SV, Weil ED, Fire Sci J. 24 (2006) 345–364.
6. Linteris GT, In: Gann RG (Ed.), Advanced Technology for Fire Suppression in Aircraft, The Final Report of the Next Generation Fire Suppression Technology Program, NIST Special Publication 1069, National Institute of Standards and Technology (2007) 119–338.
7. McDonald MA, Jayaweera TM, Fisher EM, Gouldin FC, Combust. Flame 116 (1999) 166–176.
8. Babushok VI, Tsang W, Influence of phosphorus-containing fire suppressants on flame propagation, In: Society of Fire Protection Engineers, Bethesda, MD (1999) 257–267.
9. Avondo G, Vovelle C, Delbourgo R, Combust. Flame 31 (1978) 7–16.
10. Green J, Fire Sci J. 14 (1996) 426–442.
11. Kaizerman JA, Tapscott RE, Advanced Streaming Agent Development, Volume II: Phosphorus Compounds, NMERI 96/5/32540, New Mexico Engineering Research Institute, Albuquerque, NM., 1996.
12. Hastie JW, Bonnell DW Molecular Chemistry of Inhibited combustion Systems, NBSIR 80–2169, National Bureau of Standards (1980).
13. Twarowski A, Combust. Flame 94 (1993) 91–107.
14. Werner JH, Cool TA, Kinetic Model for the Decomposition of Dmmp in a hydrogen/Oxygen Flame, Combust. Flame 117 (1999) 78–98.

15. Wainer RT, McNesby KL, Daniel RG, Miziolek AW, Babushok VI, Experimental and mechanistic investigation of opposed-flow propane/air flames by phosphorus-containing compounds, Halon Options Technical Working Conference, Albuquerque, NM, 2000, pp 141–153.
16. Glaude PA, Curran HJ, Pitz WJ, Westbrook CK, Proc. Combust. Inst 28 (2000) 1749–1756.
17. McDonald MA, Gouldin FC, Fisher EM, Combust. Flame 124 (2001) 668–683.
18. Korobeinichev OP, Bolshova TA, Shvartsberg VM, Chernov AA, Combust. Flame 125 (2001) 744–751.
19. Korobeinichev OP, Rybitskaya IV, Shmakov AG, Chernov AA, Bolshova TA, Shvartsberg VM, Proc. Combust. Inst 32 (2009) 2591–2597.
20. Korobeinichev OP, Rybitskaya IV, Shmakov AG, Chernov AA, Bolshova TA, Shvartsberg VM, Kinetics and Catalysis, 51 (2010) 154–161.
21. Bolshova TA, Korobeinichev OP, Combust. Expl. and Shock Waves, 42 (2006) 493–502.
22. Korobeinichev O, Mamaev A, Sokolov V, Bolshova T, Shvartsberg V, Zakharov L, Kudravtsev I, Inhibition of methane atmospheric flames by organophosphorus compounds, Halon Options Technical Working Conference, Albuquerque, NM, 2000, 164–172.
23. Tapscott RE, Mather JD, Heinonen EW, Lifke JL, Moore TA, Identification and Proof Testing of New Total Flooding Agents: Combustion Suppression Chemistry and Cup-Burner Testing, NMERI 97/6/33010, New Mexico Engineering Research Institute, 1998.
24. Bouvet N, Linteris GT, Babushok VI, Takahashi F, Katta VR, Krämer R, Combust. Flame 169, (2016) 340–348.
25. Shmakov AG, Korobeinichev OP, Shvartsberg VM, Knyazkov DA, Bolshova TA, Rybitskaya IV, Proc. Combust. Inst 30 (2005) 2345–2352.
26. Linteris GT, Katta VR, Takahashi F, Combust. Flame, 138 (1–2) (2004) 78–96.
27. Takahashi F, Linteris GT, Katta VR, Proc. Combust. Inst 31 (2007) 2721–2729.
28. Takahashi F, Katta VR, Linteris GT, Babushok VI, Proc. Combust. Inst 35 (2014) 2741–2748.
29. Katta VR, Goss LP, Roquemore WM, AIAA J 32 (1994) 84.
30. Roquemore WM, Katta VR, Visualization J 2, 3/4, (2000) 257–272.
31. Frenklach M, Wang H, Goldenberg M, Smith GP, Golden DM, Bowman CT, Hanson RK, Gardiner WC, Lissianski V, GRI-Mech—An optimized detailed chemical reaction mechanism for methane combustion, Report No. GRI-95/0058, Gas Research Institute, Chicago, IL, 1995.
32. Korobeinichev OP, Shvartsberg VM, Shmakov AG, Bolshova TA, Jayaweera TM, Melius CF, Pitz WJ, Westbrook CK, Proc. Combust. Inst 30 (2004) 2350–2357.
33. Takahashi F, Katta VR, Proc. Combust. Inst 28 (2000) 2071–2078.
34. Takahashi F, Linteris GT, Katta VR, Proc. Combust. Inst 31 (2007) 1575–1582.
35. Bilger RW, Proc. Combust. Inst 22 (1988) 475–488.
Newref[1]. Jayaweera TM, Melius CF, Pitz WJ, Westbrook CK, Korobeinichev OP, Shvartsberg VM, et al. “Flame inhibition by phosphorus-containing compounds over a range of equivalence ratios” Combust Flame. (2005) 140(1–2):103–115.

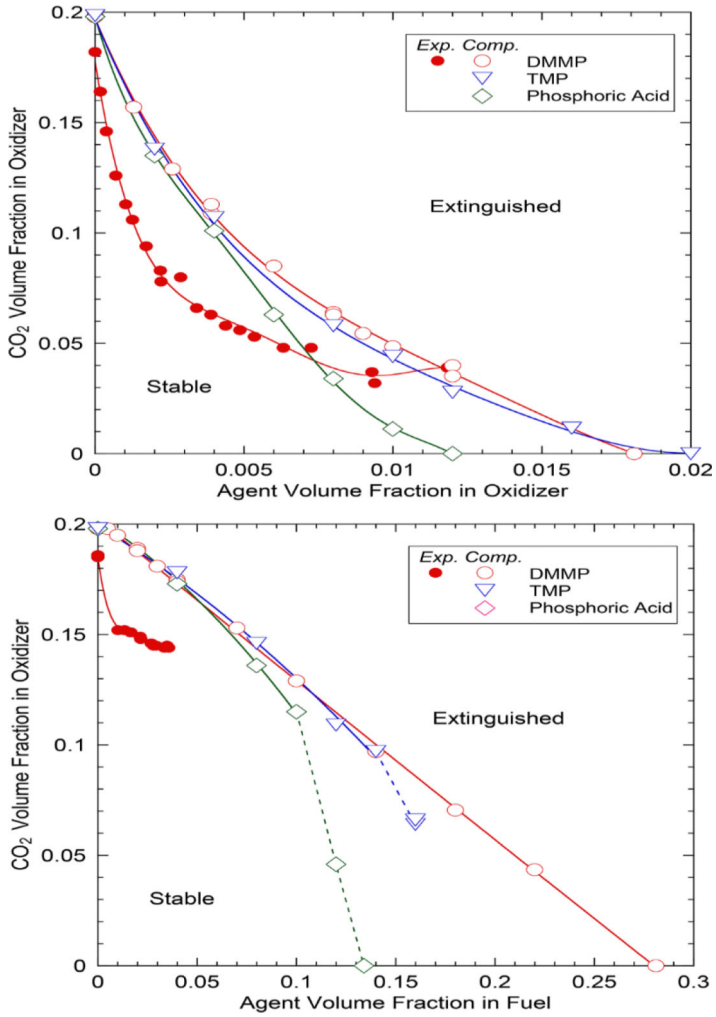

Figure 1.

Minimum extinguishing concentrations of agents in methane cup-burner flames: (a) both CO_2 and PCC added to the oxidizer and (b) CO_2 added to the oxidizer and PCC to the fuel stream.

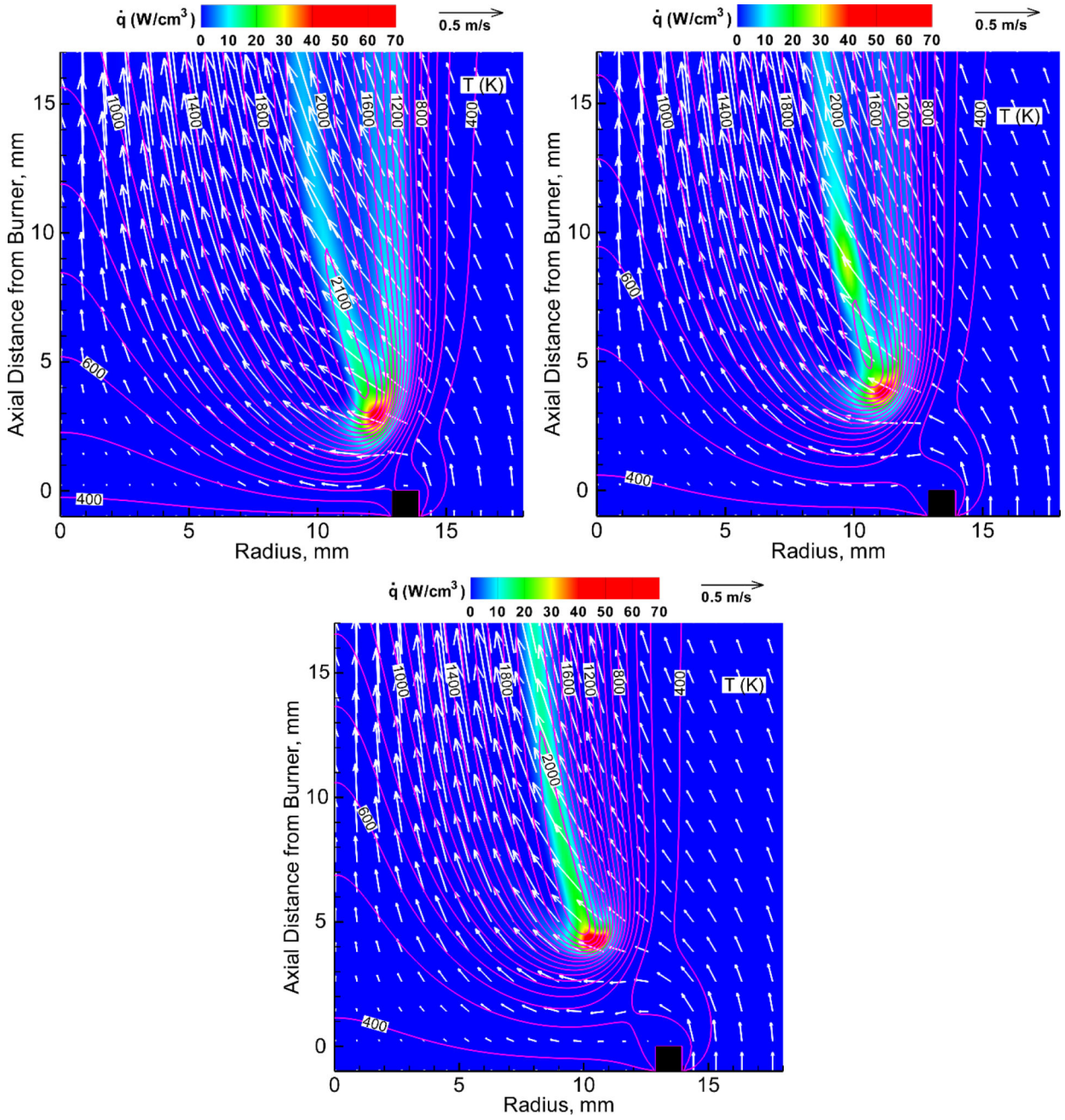

Figure 2.

Calculated structure of methane cup-burner flames in air without CO_2 and with or without agent added to the oxidizer: (a) DMMP at $X_{DMMP,OX}$=0.018, z_k=2.3 mm; (b) TMP at $X_{TMP,OX}$=0.016, z_k=3.8 mm; and (c) phosphoric acid at $X_{PO[OH]3,OX}$=0.011, z_k=4.2 mm.

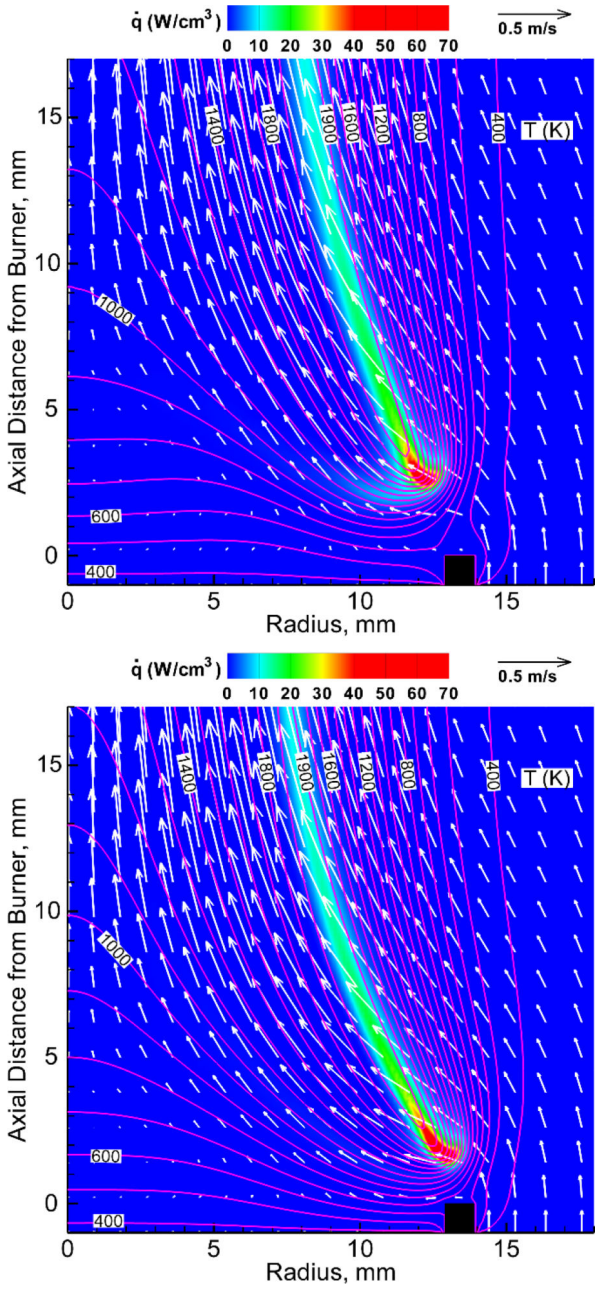

Figure 3.

Calculated structure of methane cup-burner flames in air without CO_2 and with agent added to the fuel: (a) DMMP at $X_{DMMP,FU}$=0.28, z_k=2.6 mm; and (b) phosphoric acid at $X_{PO[OH]3,FU}$=0.132, zk=1.6 mm.

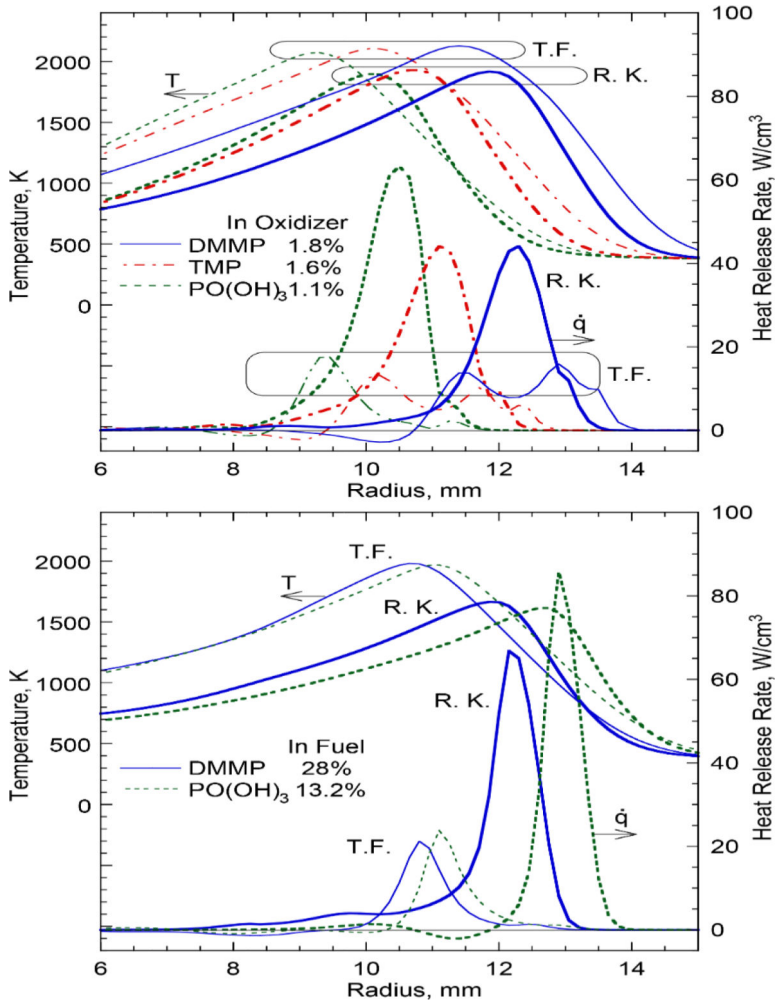

Figure 4.

Calculated radial variations of the temperature and heat-release rate crossing the reaction kernel (R.K., $z=z_k$) and the trailing flame (T.F., $z=Z_k+3$ mm) of methane cup-burner flames in air without CO_2 and with agent added to: (a) the oxidizer and (b) the fuel.

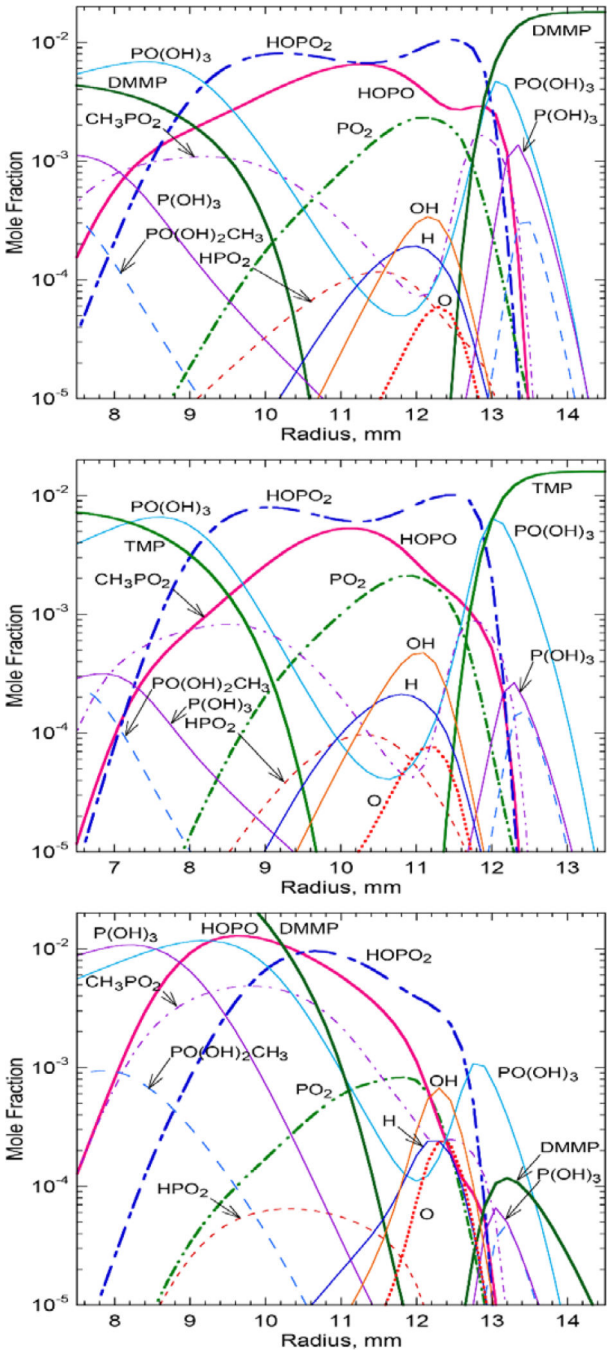

Figure 5.

Calculated radial variations of the volume fractions crossing the reaction kernel of methane cup-burner flames in air without CO_2 and with agent added to: (a)(b) the oxidizer and (c) the fuel. (a) DMMP at $X_{DMMP,OX}$=0.018, , z_k=2.3 mm; (b) TMP at $X_{TMP,OX}$=0.016, z_k=3.8 mm; and (c) DMMP at $X_{DMMP,FU}$= 0.28.

Table 1

Main radical recombination catalytic cycles by phosphorus-containing species

Catalytic Cycle	I	II
Elementary Reactions	$H + PO_2 + M \leftrightarrow HOPO + M$	
	$OH + HOPO \leftrightarrow H_2O + PO_2$	
	$H + HOPO \leftrightarrow H_2 + PO_2$	$OH + PO_2 + M \leftrightarrow HOPO_2$
	$O + HOPO \leftrightarrow OH + PO_2$	$H + HOPO_2 \leftrightarrow H_2O + PO_2$
Net Reactions	$H + H \leftrightarrow H_2$	$H + OH \leftrightarrow H_2O$
	$H + O \leftrightarrow OH$	
	$H + OH \leftrightarrow H_2O$	